IOP Publishing Journal of Physics: Condensed Matter
J. Phys.: Condens. Matter **32** (2020) 135003 (7pp) https://doi.org/10.1088/1361-648X/ab5f28

Atomic, electronic and transport properties of In–Au 2D compound on Si(1 0 0)

D V Gruznev[1], L V Bondarenko[1], A Y Tupchaya[1], V G Kotlyar[1], O A Utas[1], A N Mihalyuk[1,2], N V Denisov[1], A V Matetskiy[1,2], A V Zotov[1,2,3] and A A Saranin[1,2]

[1] Institute of Automation and Control Processes FEB RAS, 5 Radio Street, 690041 Vladivostok, Russia
[2] School of Natural Sciences, Far Eastern Federal University, 690950 Vladivostok, Russia
[3] Department of Electronics, Vladivostok State University of Economics and Service, 690600 Vladivostok, Russia

E-mail: saranin@iacp.dvo.ru

Received 16 September 2019, revised 24 November 2019
Accepted for publication 5 December 2019
Published 2 January 2020

Abstract

Two-dimensional (In, Au)/Si(1 0 0)c(2 × 2) compound was synthesized and its atomic arrangement, electron band structure and low-temperature transport properties were characterized using scanning tunneling microscopy, angle-resolved photoelectron spectroscopy and four-point-probe resistivity measurements assisted with first-principles density-functional-theory calculations. The present results are compared to those obtained earlier for the parent (Tl, Au)/Si(1 0 0)c(2 × 2) system.

Keywords: 2D compound, gold, thallium, Si(1 0 0), atomic, electronic and transport properties

(Some figures may appear in colour only in the online journal)

1. Introduction

Metal-induced reconstructions on silicon (i.e. crystalline silicon substrates covered by extra-thin ordered metal films of a thickness ranging from a fraction of a monolayer to a few monolayers) have attracted considerable interest of researchers due to abundance of fascinating structural and electronic properties. A modern trend in this field resides in the study of the multi-component systems (i.e. low-dimensional atomic-layer compounds or alloys forming upon coadsorption of two or more adsorbate species [1, 2]). This approach has been proved to be very promising for synthesis of the advanced low-dimensional materials. For example, a set of such systems (e.g. (Bi, Na)/Si(1 1 1) [3], (Tl, Sn)/Si(1 1 1) [4], (Au, Al)/Si(1 1 1) [5], etc) have been found to demonstrate a giant Rashba-type spin splitting of the metallic surface-state bands. The (Tl, Pb)/Si(1 1 1) appears to be a system where Rashba effect merges together with superconductivity [6]. The (Bi, Ag)/Si(1 1 1) [7], (In, Sb)/Si(1 1 1) [8], and (In, Bi)/Si(1 1 1) [9] systems have been shown to possess the properties of the quantum spin Hall insulators. The (Tl, Au)/Si(1 1 1) has recently been reported to be the first system which demonstrates the effect of weak antilocalization at the atomic-scale limit of film thickness [10]. It has to be admitted that most of the investigated atomic-layer compounds have been grown on the Si(1 1 1) surface. The next natural step is to expand the researches to the multi-adsorbate layers on the Si(1 0 0) substrate. Its essential difference from the Si(1 1 1) resides in a greater anisotropy due to the C_{2v} symmetry instead of the C_{3v} one of Si(1 1 1). This peculiarity has indeed been proved to affect the growth mode and properties of the grown compounds. In particular, a specific anisotropic alloying has been detected in (Ag, In)/Si(1 0 0) system [11], while an electron band structure of the (Tl, Au)/Si(1 0 0) system displays a specific spin texture with exclusively in-plane spin components which stems from the system C_{2v} symmetry [12]. Moreover, the (Tl, Au)/Si(1 0 0) compound has been reported to host two types of incommensurate charge density waves (CDWs) and exhibit the fingerprints of the one-dimensional superconductor [13].

Following this promising trend, we have addressed the (In, Au)/Si(1 0 0) system and characterized its atomic arrangement, electronic band structure and transport properties, using low-energy electron diffraction (LEED) and scanning tunneling microscopy (STM) observations, angle-resolved photoelectron spectroscopy (ARPES) and four-point-probe

 © 2020 IOP Publishing Ltd Printed in the UK

(4PP) conductivity measurements, as well as density-functional-theory (DFT) calculations. The obtained data are compared with those for the parent (Tl, Au)/Si(1 0 0) system. It has been found that both systems have the same c(2 × 2) (i.e. $\sqrt{2} \times \sqrt{2}$-R45°) periodicity and very similar atomic arrangement. Their electronic band structures have also common features. However, they differ greatly in the displayed electron transport properties at low temperatures.

2. Experimental and calculation details

The experiments on the characterization of the structural and electronic properties the samples were conducted in the UHV Omicron MULTIPROBE system equipped with LEED, STM and ARPES facilities. The electron transport measurements and low-temperature STM/STS characterization of the samples at low temperature were performed in the UNISOKU USM 1500 LT STM system, equipped with superconducting magnet and 4PP technique, which provides the lowest temperature of 1.7 K and magnetic field up to 8 T perpendicular to the sample. The base pressure in both UHV systems was on the order of 1×10^{-10} Torr. Atomically-clean two-domain Si(100)2 × 1 surface was prepared *in situ* by flashing to 1250 °C for 25 s after the sample was first annealed at 830 °C for one hour. Indium was deposited from the Ta tube and gold from the W filament. The (In, Au)/Si(1 0 0)c(2 × 2) surface was prepared by sequential adsorption of 1.0 ML (monolayer, 6.8×10^{-14} cm^{-2}) of In at 180 °C and 1.0 ML of Au at room temperature (RT) onto Si(1 0 0)2 × 1 surface followed by annealing at about 500 °C.

STM images were acquired in a constant-current mode with a mechanically cut PtIr tip after annealing in vacuum. ARPES measurements were conducted using VG Scienta R3000 electron analyzer and high-flux He discharge lamp with toroidal-grating monochromator as a light source. The 4PP head mount on the STM stage instead of the tip holder was used for the *in situ* transport measurements. Gold wires of 0.1 mm in diameter equally spaced by 0.2 mm were used for the probes.

Our calculations were based on DFT as implemented in the Vienna *ab initio* simulation package VASP [14, 15] using a planewave basis set. The projector-augmented wave approach [16] was used to describe the electron-ion interaction. The local density approximation (LDA) [17] to exchange correlation functional was employed for structure optimization and the establishment of the surface reconstruction with using *ab initio* random structure searching (AIRSS) approach [18]. To simulate the (In, Au)/Si(1 0 0) reconstructions, we used a slab consisting of forty single layers (SL) of silicon, at the LDA-optimized bulk Si lattice constant. Hydrogen atoms were used to passivate the Si dangling bonds at the bottom of the slab. The atomic positions of adsorbed atoms and atoms of Si layers within the six SLs of the slab were optimized. Silicon atoms of the deeper layers were kept fixed at the bulk crystalline positions. The geometry optimization was performed until the residual force on atoms was smaller than 10 meV Å^{-1}. For band structure calculations we used LDA functional approach. Within LDA we applied an approximate quasiparticle approach LDA-1/2 [19, 20] to improve the Si band gap. The kinetic cutoff energy was 250 eV, and a 12 × 12 × 1 *k*-point mesh was used to sample the surface Brillouin zone.

3. Results and discussion

3.1. Atomic arrangement

Morphological and structural arrangement of the (In, Au)/Si(1 0 0)c(2 × 2) surface is illustrated in figure 1, where figures 1(a) and (b) show large-scale and high-resolution STM images, respectively. One can see that the surface is principally flat and homogeneous, but contains scarce surface defects, bright features which are associated with minute excess of Au atoms and dark trenches which origin remains unclear and their formation might be caused by relieving the surface stress in the adsorbate layer. Both types of defects were always present at the sample surface. Minimal density of the bright defects achieved by optimization of the growth conditions was about 4×10^{12} cm^{-2}. Nevertheless, the surface exhibited a well-defined long-range ordering as indicated by observation of a sharp and bright c(2 × 2) LEED pattern (see inset in figure 1(a)).

The first-principles DFT calculations were performed to determine an atomic structure of the (In, Au)/Si(1 0 0)c(2 × 2) surface. It was found that the lowest-energy (In, Au)/Si(1 0 0) configuration contains 1.0 ML of In and 1.0 ML of Au and its atomic structure is akin that established recently for the (Tl, Au)/Si(1 0 0)c(2 × 2) surface [12] (figure 1(c)), namely, this is a double-atomic-layer In/Au/Si(1 0 0) structure where Au atoms (shown by yellow balls in figure 1(c)) form the bottom layer which resides on the bulk-like truncated Si(1 0 0) surface, while the top layer is composed of In (Tl) atoms (blue balls in figure 1(c)). A close correspondence between experimental and simulated STM images (figure 1(d)) provides a strong support for the validity of the proposed model of the (In, Au)/Si(1 0 0)c(2 × 2) structure.

The structures of (In, Au)/Si(1 0 0) and (Tl, Au)/Si(1 0 0) compounds are similar but differ quantitatively in the particular structural parameters (see table 1). As compared to the Tl–Au double layer, the In–Au layer is more compressed in vertical direction ($h^{\mathrm{In-Au}} = 1.04$ Å versus $h^{\mathrm{Tl-Au}} = 1.54$ Å) and is more distant from Si(1 0 0) substrate ($h^{\mathrm{Au-Si}}$ equals 2.48 Å for (In, Au)/Si(1 0 0) and 1.42 Å for (Tl, Au)/Si(1 0 0)). Another essential difference resides in the extent of dimerization within the atomic layers which is greatly expressed in the (In, Au)/Si(1 0 0) compound. In the (Tl, Au)/Si(1 0 0), the Au layer exhibits only a motif for dimerization (the nearest Au–Au distance of 3.30 Å noticeably exceeds the bulk Au–Au value of 2.88 Å), while the Tl layer shows a more clear dimerization with Tl–Tl distance of 3.44 Å which is close to the bulk value, 3.40 Å. In contrast, the (In, Au)/Si(1 0 0) is dimerized in the both, In and Au layers, as its nearest Au–Au distance of 2.98 Å almost coincides with the bulk value 2.88 Å, while the In–In distance is even less than the bulk value (3.10 Å versus 3.34 Å).

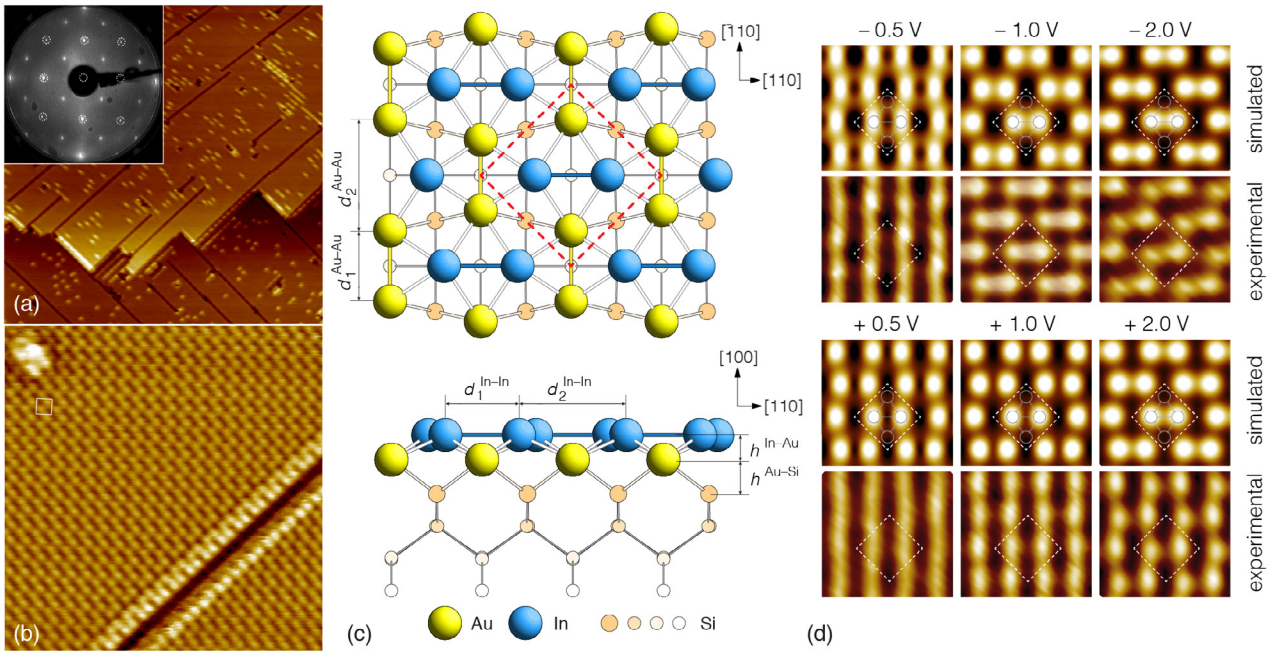

Figure 1. (a) Large-scale ($100 \times 100\,nm^2$) filled-state ($-2.0\,V$) and (b) high-resolution ($11 \times 11\,nm^2$) empty-state ($+2.0\,V$) STM images of (In, Au)/Si(100)c(2 × 2) surface. Inset in (a) shows LEED pattern ($E_p = 83\,eV$) from the surface. (c) Structural model of the (In, Au)/Si(100)c(2 × 2) where yellow balls are for Au atoms, blue balls for In atoms and orange circles of different size and contrast for Si atoms in various layers. (d) Comparison of experimental and simulated empty-state STM images for $-0.5\,V$, $-1.0\,V$ and $-2.0\,V$ sample bias voltages (upper panel) and filled-state STM images for $+0.5\,V$, $+1.0\,V$ and $+2.0\,V$ sample bias voltages (lower panel). The $\sqrt{2} \times \sqrt{2}$-R45° primitive cell is outlined by red hatched square in (c) and by white hatched squares in (b) and (d).

3.2. Electronic band structure

Figure 2 shows electron band structure calculated for the proposed (In, Au)/Si(100)c(2 × 2) model without and with spin orbit coupling (SOC) contribution being included (figures 2(a) and (b), respectively). Figure 3 shows the calculated Fermi-contour map. Comparison of these data with those for the (Tl, Au)/Si(100)c(2 × 2) surface [12] reveals that electron band structures of the two systems have much in common. In the both systems, the main features are the two metallic surface-state bands, denoted S_1 and S_2. Both bands are spin-split and their peculiar feature is a presence of only the in-plane spin components that stems from the C_{2v} symmetry of the systems [12]. The S_2 has a vortical spin texture, hence a zero net spin for the corresponding Fermi contours, while S_1 demonstrates unusual nonvortical spin texture with a non-zero net spin for the corresponding Fermi contours (indicated by solid red and blue arrows in figure 3). Worth noting is that even the shapes of the band dispersions in (In, Au)/Si(100) and (Tl, Au)/Si(100) systems are very similar and the main difference resides in the different electron filling of the bands and position of the Fermi level. In the (In, Au)/Si(100) the electron density is slightly greater than that in the (Tl, Au)/Si(100) ($7.44 \cdot 10^{14}\,cm^{-2}$ versus $6.93 \cdot 10^{14}\,cm^{-2}$) and the Fermi level is shifted upward. The latter is clearly seen if one compares the Fermi-contour maps for the two systems (see figure 3, where the sketch of the Fermi-contour map for the (Tl, Au)/Si(100) is shown in the inset in the right-up corner). In the (Tl, Au)/Si(100) system, the contours of the spin-split hole S_1 band have a shape of elongated bean pods, but they change to individual 'beans' in the Fermi-contour map of the (In, Au)/Si(100), as a result of the upward shifting of the Fermi level.

As an additional check for the (In, Au)/Si(100)c(2 × 2) surface model, the band structure calculations were compared with the experimental ARPES data (figure 4). For a proper comparison, one should bear in mind that the (Tl, Au)/Si(100) c(2 × 2) compound occurs in the two domain orientations, since the Si(100) surface structure is rotated by 90° when crossing each atomic step. Therefore, the ARPES spectrum reflects the superposition from the two rotational domains. In the present work, the ARPES spectra were recorded along the $\overline{\Gamma}$-$\overline{X}$ direction, where two domains contribute equally, and along the $\overline{\Gamma}$-$\overline{M}$ directions, where their contributions are different (see figures 2 and 3). In the resultant ARPES spectrum, the two inequivalent contributions along the $\overline{\Gamma}$-$\overline{M}$ and $\overline{\Gamma}$-$\overline{M}'$ directions are superimposed. In the calculated band structure the $\overline{\Gamma}$-$\overline{M}$ and $\overline{\Gamma}$-$\overline{M}'$ directions were also overlayed. One can see that coincidence between experimental and calculated spectra is fairly good. Correspondence between characteristic features in the experimental and calculated Fermi-contour maps is also apparent (figure 5). All these together can serve as solid arguments for a correctness of the present (In, Au)/Si(100)c(2 × 2) structural model.

3.3. Low-temperature transport properties

Figure 6 shows the temperature dependence of the sheet resistance of the (In, Au)/Si(100)c(2 × 2). The sample resistance amounts to 2–3 times larger than the resistance quantum

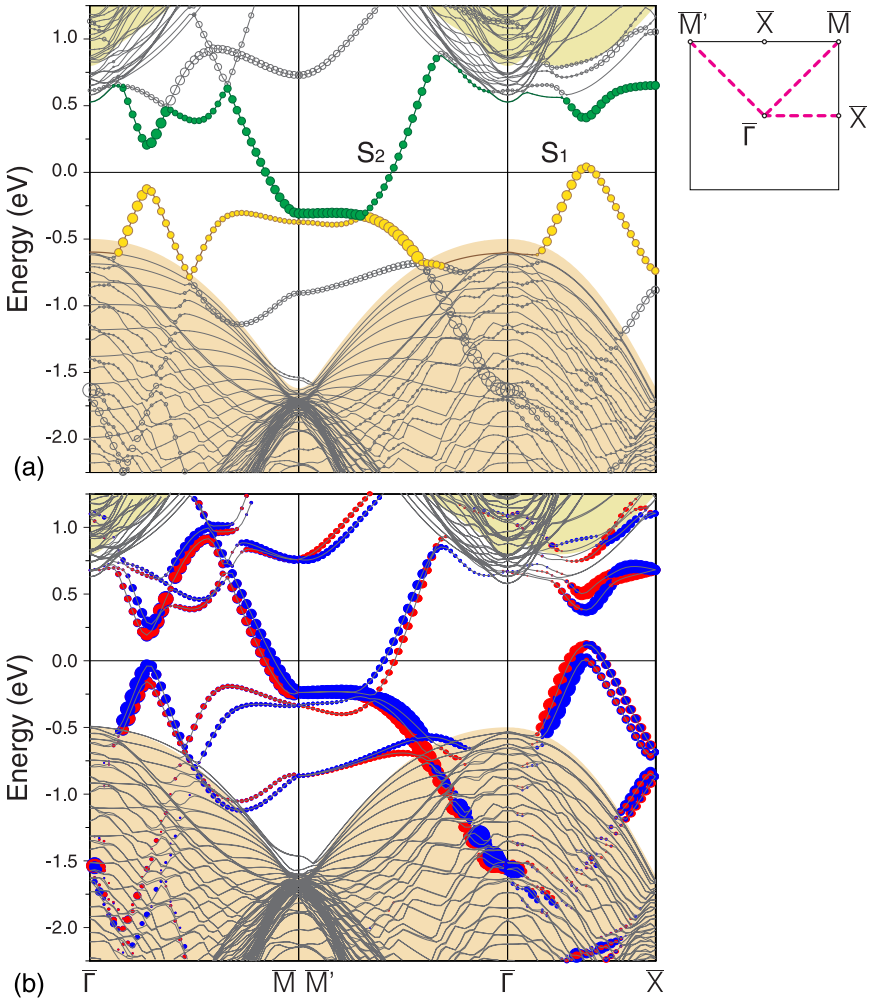

Figure 2. Calculated electron band structure of the (In, Au)/Si(1 0 0)c(2 × 2) surface (a) without and (b) with SOC contribution taken into account. The metallic surface-state bands, S_1 and S_2, are highlighted in (a) by the yellow and green circles, respectively. The bands with opposite spin orientation are highlighted in (b) by the red and blue circles. The size of the circle corresponds to the strength of the surface character. Hatched region shows the projected bulk bands. The right panel presents the $\sqrt{2} \times \sqrt{2}$ SBZ with indicated high-symmetry points together with the passes along which the dispersions were calculated.

Table 1. Structural parameters of the $\sqrt{2} \times \sqrt{2}$-(In, Au) and $\sqrt{2} \times \sqrt{2}$-(Tl, Au) 2D compounds on Si(1 0 0) substrate. All values are in Å units. Bulk $d^{\text{In–In}} = 3.34$ Å, $d^{\text{Tl–Tl}} = 3.40$ Å and $d^{\text{Au–Au}} = 2.88$ Å. For the meaning of parameters see figure 1 (c).

System	$h^{\text{In(Tl)–Au}}$	$h^{\text{Au–Si}}$	$d_1^{\text{Au–Au}}$	$d_2^{\text{Au–Au}}$	$d_1^{\text{In–In(Tl–Tl)}}$	$d_2^{\text{In–In(Tl–Tl)}}$
(In, Au)	1.04	2.48	2.98	4.65	3.10	4.53
(Tl, Au)	1.57	1.42	3.30	4.43	3.44	4.28

($h/e^2 = 25.813$ kΩ) at ∼ 30 K and rapidly grows with decreasing temperature indicating the strong localization. In the 2D case, variable-range hopping of the form $\rho \propto \exp[(1/T)^{1/3}]$ was predicted by Mott [21] assuming that the DOS near the Fermi level is constant. Lowering the temperature usually results in the Efros–Shklovskii mechanism with $\rho \propto \exp[(1/T)^{1/2}]$ for a parabolic gap [22]. More generally, Pollak [23] and Hamilton [24] showed that for the DOS varying as $|E - E_F|^m$ the resistivity is given by $\rho = \rho_0 \cdot \exp[(T_0/T)^x]$ with an exponent $x = (m + 1)/(m + 3)$ in the 2D case. Though an exponent of 1/2 has been found for many systems, at low temperatures a more stronger temperature dependence of resistivity occurs with an exponent x larger than 1/2 [25]. Fitting of our data yields the exponent values of $x = 0.58$ and $x = 0.95$ for high and low temperature ranges, respectively (figure 6), which are about twice greater than one could expect for the Mott and Efros–Shklovskii regimes. To resolve this discrepancy, a more sophisticated theoretical considerations are believed to be required.

In general, the low-temperature transport properties of the (In, Au)/Si(1 0 0)c(2 × 2) differ from those of the parent (Tl, Au)/Si(1 0 0)c(2 × 2) system. In case of the (Tl, Au)/Si(1 0 0)c(2 × 2), the results of the transport measurements are strongly affected by the density of surface defects of vacancy type, associated with Tl deficit [13]. With minimal density of defects of $\sim 10^{12}$ cm^{-2}, the (Tl, Au)/Si(1 0 0) sample has a resistance of ∼2 kΩ and upon cooling it exhibits fingerprints

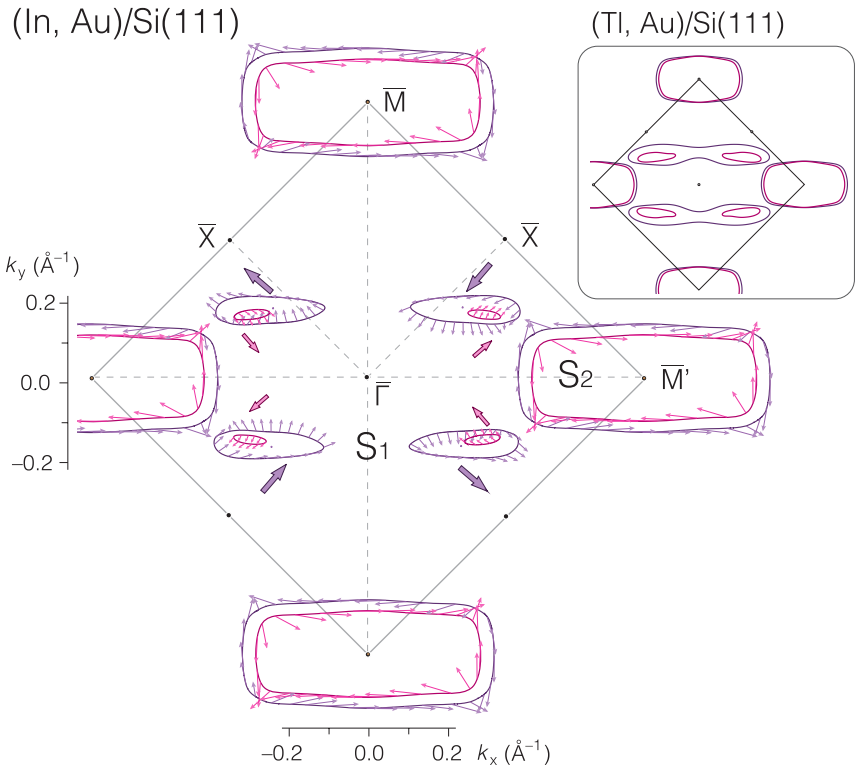

Figure 3. Calculated Fermi-contour map of the (In, Au)/Si(1 0 0)c(2 × 2) surface where blue and red arrows adjacent to the contours and their length denote the in-plane spin component. The net spin for each Fermi contour of S_1 band is shown by bold blue and red arrows. The $\sqrt{2} \times \sqrt{2}$ SBZ is outlined. Inset in the right-up corner shows for comparison a sketch of the Fermi-contour map of the (Tl, Au)/Si(1 0 0)c(2 × 2) surface.

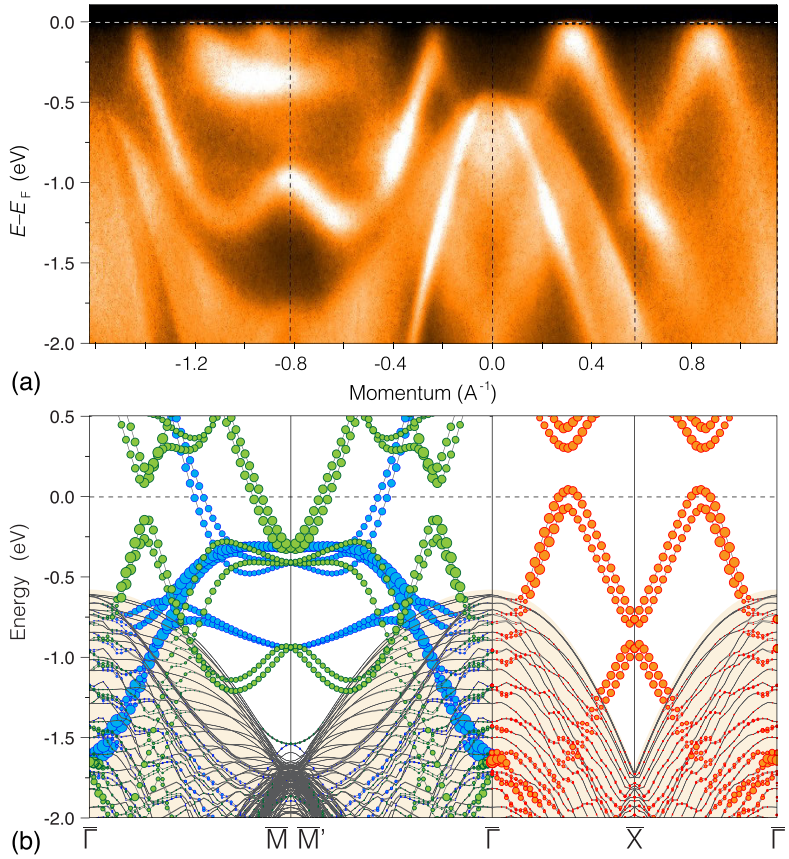

Figure 4. Comparison of the (a) experimental ARPES spectrum with (b) calculated band structure of the (In, Au)/Si(1 0 0)c(2 × 2) surface. In (b) the contributions from the inequivalent $\overline{\Gamma}$-$\overline{M}$ and $\overline{\Gamma}$-$\overline{M}'$ directions are superposed and corresponding dispersions are shown by green and blue circles. Orange circles denote the dispersion along the $\overline{\Gamma}$-$\overline{X}$ direction where the contributions from the two domains are identical.

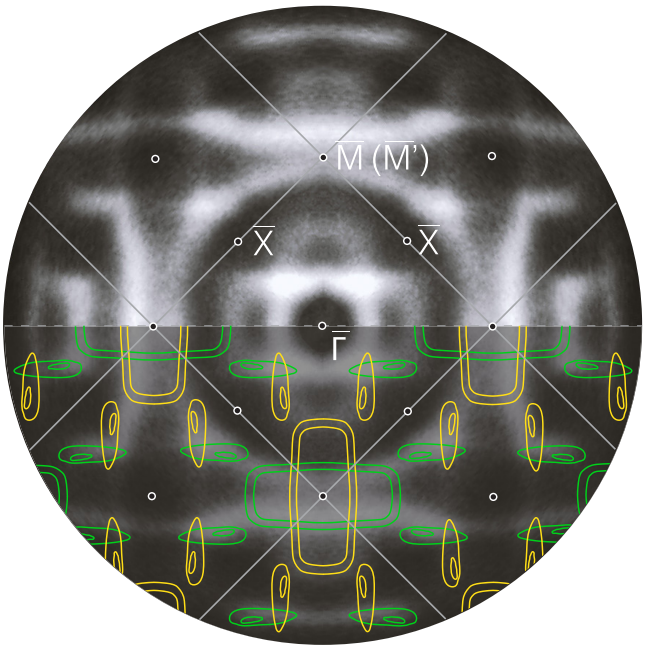

Figure 5. Experimental and calculated Fermi-contour maps of the (In, Au)/Si(1 0 0)c(2 × 2) surface shown in the upper and lower panels, respectively. Grey lines indicate the $\sqrt{2} \times \sqrt{2}$ SBZs boundaries. The calculated contours originated from the two rotational domains are highlighted by yellow and green colors.

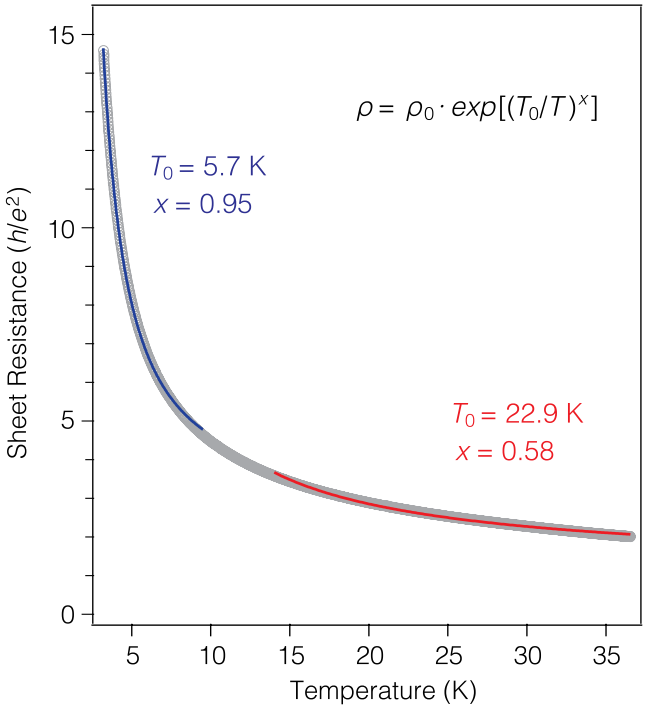

Figure 6. (a) Temperature dependence of the sheet resistance of the (In, Au)/Si(1 0 0)c(2 × 2) sample. Grey symbols are experimental data, red and blue lines show the data fitting in the two temperature ranges. The least-square fitting values are indicated.

of a one-dimensional superconductor with a critical temperature $T_c = 1.33$ K. When the density of defects is relatively high, i.e. on the order of $\sim 6 \cdot 10^{12}$ cm^{-2}, the sample resistance is $\sim$15 kΩ and upon cooling the sample transfers into the insulator state. In the present case of (In, Au)/Si(1 0 0)c(2 × 2), the defects are of the other types and we were unable to vary their density, in particular to decrease the density of bright defects, associated with excess Au, below the $\sim 4 \cdot 10^{12}$ cm^{-2} level, which is slightly lower than density of defects in the 'defective' (Tl, Au)/Si(1 0 0)c(2 × 2) samples. Nevertheless, resistance of the (In, Au)/Si(1 0 0)c(2 × 2) samples was essentially greater, $\sim$50 kΩ, possibly due to a presence of linear defects seen as dark trenches in the STM images.

4. Summary

In conclusion, using LEED, STM, ARPES and *in situ* 4PP transport measurements in combination with the DFT calculations we characterized the structural and electronic properties of the (In, Au)/Si(1 0 0)c(2 × 2) 2D compound and compared them with those of the parent (Tl, Au)/Si(1 0 0)c(2 × 2) system. Both (In, Au) and (Tl, Au) compounds have a basically similar double-atomic-layer structure where 1.0 ML of Au atoms constitutes the bottom layer which resides on the bulk-like truncated Si(1 0 0) surface, while the top layer is built of 1.0 ML of In (Tl) atoms. The structural difference resides in the extent of dimerization within the atomic layers which is greatly expressed in the (In, Au)/Si(1 0 0) compound making its structure more rigid. Electronic band structures of the two systems have also much in common. They contain two metallic spin-split surface-state bands. The characteristic feature of their spin texture is occurrence of only in-plane spin component. One of the two bands has a typical vortical spin texture, while the other exhibits unusual nonvortical spin texture. The difference in the electronic structures resides in the electron filling of the surface-state bands which is slightly greater in the (In, Au)/Si(1 0 0) as compared with the (Tl, Au)/Si(1 0 0): $7.44 \cdot 10^{14}$ cm^{-2} versus $6.93 \cdot 10^{14}$ cm^{-2}. The greatest difference between the two systems concerns the low-temperature transport properties. While the 'perfect' (Tl, Au)/Si(1 0 0) system demonstrates superconducting behavior, the (In, Au)/Si(1 0 0) system always exhibits transition into insulator state. This result indicates that occurrence of superconductivity in the atomic-layer systems is highly sensitive to the minute variations in their atomic and electronic properties, as well as type and density of surface defects. We believe that the comprehensive information on the structural and electronic properties gained in our studies for the (In, Au)/Si(1 0 0) and (Tl, Au)/Si(1 0 0) systems might provide a useful basis for explicit theoretical understanding of this and related phenomena.

Acknowledgments

The work was supported by the Russian Science Foundation under Grant 19-12-00101. The calculations were conducted using the equipment of Shared Resource Center 'Far Eastern Computing Resource' IACP FEB RAS (https://cc.dvo.ru) and were partially supported by RFBR Grant 18-52-52012.

ORCID iDs

A N Mihalyuk https://orcid.org/0000-0003-4483-2207
A V Matetskiy https://orcid.org/0000-0002-4967-604X
A A Saranin https://orcid.org/0000-0001-6642-2466

References

[1] Osiecki J R, Sohail H M, Eriksson P E J and Uhrberg R I G 2012 *Phys. Rev. Lett.* **109** 057601
[2] Gruznev D V, Zotov A V and Saranin A A 2017 *Japan. J. Appl. Phys.* **56** 08LA01–8
[3] Zhou M, Ming W, Liu Z, Wang Z, Yao Y and Liu F 2014 *Sci. Rep.* **4** 7102–6
[4] Gruznev D V, Bondarenko L V, Matetskiy A V, Tupchaya A Y, Alekseev A A, Hsing C R, Wei C M, Eremeev S V, Zotov A V and Saranin A A 2015 *Phys. Rev.* B **91** 035421
[5] Gruznev D V, Bondarenko L V, Matetskiy A V, Tupchaya A Y, Chukurov E N, Hsing C R, Wei C M, Eremeev S V, Zotov A V and Saranin A A 2015 *Phys. Rev.* B **92** 245407
[6] Matetskiy A V, Ichinokura S, Bondarenko L V, Tupchaya A Y, Gruznev D V, Zotov A V, Saranin A A, Hobara R, Takayama A and Hasegawa S 2015 *Phys. Rev. Lett.* **115** 147003
[7] Zhang X, Cui B, Zhao M and Liu F 2018 *Phys. Rev.* B **97** 085422
[8] Gruznev D V, Eremeev S V, Bondarenko L V, Tupchaya A Y, Yakovlev A A, Mihalyuk A N, Chou J P, Zotov A V and Saranin A A 2018 *Nano Lett.* **18** 4338–45
[9] Hsu C H, Huang Z Q, Lin C Y, Macam G M, Huang Y Z, Lin D S, Chiang T C, Lin H, Chunag F C and Huang L 2018 *Phys. Rev.* B **98** 121404
[10] Matetskiy A V, Denisov N V, Zotov A V and Saranin A A 2019 *Nano Lett.* **19** 570–5
[11] Sobotík P, Kocán P and Oăstádal I 2018 *Surf. Sci.* **677** 8–11
[12] Gruznev D V, Bondarenko L V, Tupchaya A Y, Kotlyar V G, Utas O A, Mihalyuk A N, Eremeev S V, Zotov A V and Sranin A A 2018 *Phys. Rev.* B **98** 125428
[13] Denisov N V, Matetskiy A V, Mihalyuk A N, Eremeev S V, Hasegawa S, Zotov A V and Saranin A A 2019 *Phys. Rev.* B **100** 155412
[14] Kresse G and Hafner J 1993 *Phys. Rev.* B **47** 558
[15] Kresse G and Joubert D 1999 *Phys. Rev.* B **59** 1758
[16] Blöchl P E 1994 *Phys. Rev.* B **50** 17953–79
[17] Perdew J P and Zunger A 1981 *Phys. Rev.* B **23** 5048–79
[18] Pickard C J and Needs R J 2011 *J. Phys. Condens. Matter* **23** 053201
[19] Ferreira L G, Marques M and Teles L K 2008 *Phys. Rev.* B **78** 125116
[20] Ferreira L G, Marques M and Teles L K 2011 *AIP Adv.* **1** 032119
[21] Mott N F 1968 *J. Non-Cryst. Solids* **1** 1–17
[22] Efros A L and Shklovskii B I 1975 *J. Phys. C: Solid State Phys.* **8** L49–51
[23] Pollak M 1972 *J. Non-Cryst. Solids* **11** 1–24
[24] Hamilton E M 1972 *Phil. Mag.* **26** 1043–5
[25] Dai P, Zhang Y and Sarachik M P 1992 *Phys. Rev. Lett.* **69** 1804–6